Multiscale Modeling of Protein Adsorption and Transport in Macroporous and Polymer-Grafted Ion Exchangers

Joseph E. Basconi, Giorgio Carta, and Michael R. Shirts
Dept. of Chemical Engineering, University of Virginia, Charlottesville, VA

DOI 10.1002/aic.14621
Published online September 30, 2014 in Wiley Online Library (wileyonlinelibrary.com)

A multiscale model is presented to elucidate protein adsorption and transport behaviors in ion-exchange chromatography (IEC) adsorbent particles that have either an open pore structure or charged dextran polymers grafted into the pores. Molecular dynamics simulation is used to determine protein diffusion and partitioning in different regions of the adsorbent pore, and these outputs are used in numerical simulations of mass transfer to determine the intraparticle protein concentration profile and the mass-transfer rate. Modeling results indicate that, consistent with experimental observations, protein transport can be faster in the polymer-grafted material compared to the open pore case. This occurs when favorable partitioning of protein into the polymer-filled pore space is combined with relatively high protein mobility within this region. The modeling approach presented here should be applicable to proteins and adsorbents with different properties, and could help elucidate the factors that control adsorption and transport in various IEC systems.
 AIChE J, 60: 3888–3901, 2014
Keywords: protein chromatography, absorption, ion-exchange, molecular dynamics, multiscale modeling

Introduction

Ion-exchange chromatography (IEC) is used extensively to separate and purify proteins for pharmaceutical applications.[1] In this process, protein mixtures are separated based on the differing electrostatic interactions between protein molecules and charged ligands bound to a support matrix. Traditional matrices for IEC consist of macroporous particles. In these systems, the protein binding capacity is limited by the macropore surface area while protein transport occurs by ordinary diffusion in the liquid-filled pores. Because the pore size has to be relatively large to prevent excessive diffusional hindrance, the protein binding capacity is typically relatively small.[2]

Polymer-grafted ion exchangers have been developed in recent years with the intent of increasing protein binding capacities and mass-transfer rates.[3–6] In these systems, flexible polymers are grafted to the pore surfaces of a macroporous support matrix. When functionalized with charged groups, the polymers are thought to extend into the bulk of the pores creating a separate phase, akin to a hydrogel, allowing protein binding throughout the pore volume rather than only at the surface.

Stone and Carta studied the adsorption behavior of different proteins on cation exchangers consisting of porous agarose particles with either an open pore structure or with dextran polymers functionalized with sulfonate charged groups grafted to the pore surfaces.[5] In both materials, the underlying agarose matrix was also functionalized with sulfonate groups. In single-component adsorption experiments, the binding capacities of lysozyme and IgG were 15 and 25% higher, respectively, in the dextran-grafted matrix than in the open pore material.[5,7] The rate of adsorption was also determined for these proteins from batch adsorption experiments. An apparent effective pore diffusivity, $D_{e,app}$, was obtained by fitting the batch uptake curves to a pore diffusion model, in which transport occurs only via the diffusion of unadsorbed protein within the pore liquid. While low values of $D_{e,app}$ were obtained for the open-pore adsorbent, consistent with hindered diffusion in the particle macropores, surprisingly high values of $D_{e,app}$ which in some cases even exceeded the protein molecular diffusivity in solution, D_0, were obtained for the dextran-grafted adsorbent. This initially paradoxical finding was explained by the possibility that protein molecules interacting with the charged polymer grafts retain diffusional mobility. Since the concentration of these molecules is expected to be higher than in free solution as a result of favorable electrostatic interactions with the charged polymers, transport occurs faster in the polymer-grafted media compared to the macroporous one because of the larger driving force due to the higher concentration gradient. For conditions where protein binding is highly favorable, the following relationship can be used to relate $D_{e,app}$ to the diffusivity, D', of the bound protein molecules[2,5]

$$D_{e,app} \sim D' \frac{q^*}{C} \tag{1}$$

where q^* is the total adsorbed protein concentration at equilibrium and C the protein concentration in solution. This equation does not distinguish between protein molecules interacting with the dextran polymers (which could be expected to be

Additional Supporting Information may be found in the online version of this article.

Correspondence concerning this article should be addressed to M. R. Shirts at michael.shirts@virginia.edu.

relatively mobile), and those interacting with the underlying surface of the support matrix. Thus, D' is an effective molecular diffusivity incorporating the differing behaviors of protein molecules on and off of the pore surface.

Although there is considerable macroscopic and microscopic experimental evidence that charged polymer grafts can enhance both protein binding capacities and mass-transfer rates as compared to those found in open pore matrices, the molecular details of adsorption and transport in these polymer-grafted matrices remain elusive.[8] For example, different types of proteins have exhibited significant variations in the extent to which $D_{e,app}$ is enhanced in a dextran-grafted material, and in the range of ionic strength at which the enhancements are observed.[7] The reasons for these differences are not fully understood, but presumably depend on the molecular properties of the protein and adsorbent, and how they interact. A detailed understanding of how these properties affect macroscopic adsorption behaviors is necessary to tailor the adsorbent synthesis and operating conditions to achieve efficient separations of proteins with different characteristics.

Various multiscale models have been used to study protein adsorption in macroporous materials as a function of molecular-level details.[9] Lenhoff has developed a model applicable to IEC systems governed by a parallel diffusion mechanism (in which proteins diffuse on the pore surface as well as within the pore fluid), that predicts the apparent pore diffusivity based on adsorbent structural properties, protein size and binding capacity, operating conditions, and chromatographic retention.[10] The model predicts a significant increase in $D_{e,app}$ of lysozyme in a commercial macroporous adsorbent as the salt concentration is increased. This trend is consistent with experiments by Dziennik et al. for lysozyme adsorption in the cation exchanger SP Sepharose FF.[11] However, it is inconsistent with the results of Ubiera and Carta who found a constant diffusivity of $D_{e,app} = 1.8 \pm 0.3 \times 10^{-7}$ cm^2/s for the same system at ionic strengths between 0.02 and 0.12 M.[12] The reasons why the results of Dziennik et al. and those of Ubiera and Carta are different are not known. One possibility is that Dziennik et al. used a batch method where the protein solution concentration varied and the kinetics were determined by material balance, while Ubiera and Carta used a radiotracer method which provided direct measurements at a constant protein concentration. Ubiera and Carta also found that $D_{e,app}$ of lysozyme decreases rather than increases with ionic strength in the cation exchanger SP Sepharose XL, which has the same backbone matrix as SP Sepharose FF but contains charged grafted dextran polymers.[12] Riccardi et al. also used multiscale modeling to predict intraparticle protein concentration profiles in an adsorbent governed by ordinary pore diffusion, based on molecular dynamics (MD) simulation results for the spatial distribution of charged ligands immobilized within the adsorbent. In addition to these multiscale studies, MD has been used extensively to study the structural and energetic details of peptide and protein molecules interacting with various types of chromatography adsorbents and ligands,[13,14] including charged surfaces,[15–18] charged polymers,[19,20] and multimodal chromatography ligands.[21]

While the multiscale models described above are applicable to macroporous adsorbents, a more generalizable approach is needed to predict protein adsorption in complex systems for which the underlying transport mechanism is not well understood, such as polymer-grafted adsorbents. In this work, we present a multiscale model for studying adsorption behaviors in IEC systems with different pore architectures based on molecular-level details. The approach includes MD simulation used to study the diffusion and partitioning of protein molecules in different locations within an adsorbent pore. From this partitioning behavior, the adsorption equilibria can be predicted. The modeling uses numerical simulation of mass transfer to predict the adsorption kinetics over experimentally relevant length and time scales as a function of the molecular behaviors observed from MD.

This article focuses on two objectives directed toward developing the multiscale model. The first is to determine how the molecular behaviors of the protein interacting with the adsorbent affect the overall adsorption kinetics. The second is to determine which molecular details of the model lead to macroscopic adsorption behaviors that are consistent with the experimental results described above for lysozyme in macroporous and dextran-grafted IEC particles.[5] This work takes initial steps toward being able to predict adsorption behaviors as a function of the protein and adsorbent's molecular-level details, for macroporous as well as polymer-grafted ion exchangers.

Methods

Development of molecular models

We perform MD simulations of protein molecules in both an open macropore and a polymer-grafted pore environment to determine the diffusion and partitioning of the protein based on the system's molecular-level properties. A coarse-grained (CG) approach in which multiple atoms are lumped into individual interaction sites (or "beads") is used to efficiently simulate large ensembles of protein molecules to measure diffusivities and partitioning behaviors with low statistical error. Rather than deriving the CG model from a more detailed atomistic model, we use a hypothesis-driven approach, in which we include in the model only the components and interactions that we hypothesize control the protein–adsorbent interactions that govern macroscopic adsorption behaviors. The components are the lysozyme protein molecules, the sulfonate charged groups on the agarose pore surfaces, and the charged dextran grafts (for the polymer-grafted system). Figure 1 shows snapshots from MD simulations of the macroporous and polymer-grafted systems. Explicit water molecules and solution ions are not included, however, their effects on molecular diffusion and electrostatic interactions are represented implicitly, as discussed in the next section.

The approach used to parameterize the model's molecular details depends on the relative uncertainty in our information about these details. Details describing intrinsic material properties that are known with relatively low uncertainty are parameterized to reproduce these properties as directly as possible. For example, the size and structure of the protein molecule are parameterized based on the protein's crystal structure, under the assumption that the crystal structure is an appropriate approximation for the native structure in solution.

Model details that are not directly constrained by experimental data, such as the density of charged groups on the surface, the charge content of grafted polymers, and the strength of electrostatic interactions under favorable binding

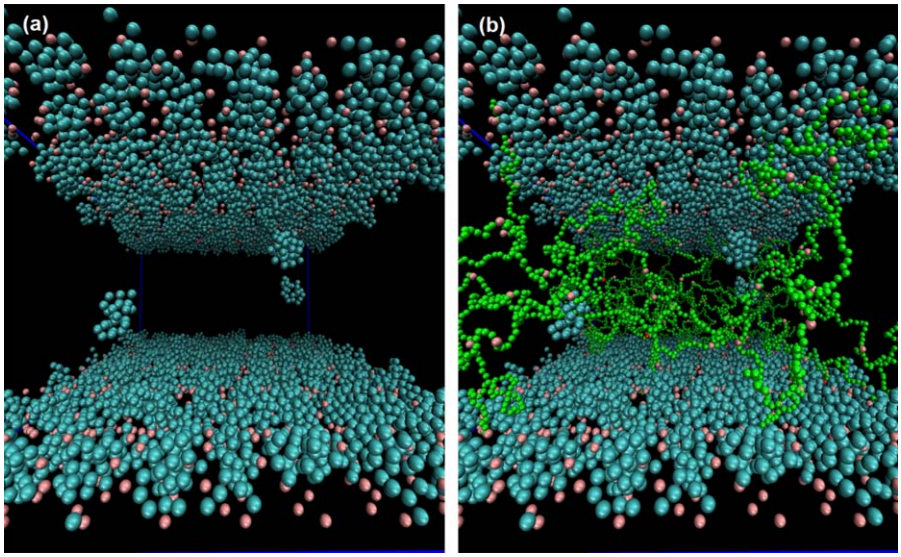

Figure 1. Snapshots from equilibrated MD simulations of lysozyme within an idealized pore of a cation-exchange particle, with either an open pore structure (a), or with charged dextran polymers grafted onto the pore surface (b).

Both adsorbents are near saturation. Lysozyme, dextran, and sulfonate groups are shown in blue, green, and pink, respectively. [Color figure can be viewed in the online issue, which is available at wileyonlinelibrary.com.]

conditions are tuned such that the model predicts adsorption behaviors that agree qualitatively with the following experimental behaviors for lysozyme under favorable binding conditions:

1. a monolayer surface coverage of bound protein in the macroporous system,
2. mass transfer controlled by diffusion in the liquid contained within the pore in the macroporous system (such that $D_{e,app}/D_0 \approx 1$), and
3. an enhancement in $D_{e,app}/D_0$ for the polymer-grafted system.

The first criterion relates to the adsorption equilibria and is suggested by the fact that experimental adsorption equilibria are consistent with the Langmuir adsorption model, while the latter two criteria are related to both the adsorption equilibria and kinetics.

The use of a CG model, an implicit representation of the solvent, and simple interaction potentials improves the computational efficiency of the MD simulations by approximately four orders of magnitude as compared to using a model with full atomistic detail. For example, on a standard 8-core desktop, a simulation of a CG model of the polymer-grafted pore and a high protein loading ran at 0.16 h/ns, while an atomistic simulation of approximately 1.3 million water molecules (which would comprise most of the overall computation cost) with the same box dimensions used for the CG case ran at 1600 h/ns. All MD simulations were performed using GROMACS version 4.6.4.[22] The following sections describe details of the molecular modeling.

Solvent environment

The simulations are performed in the NVT (constant number of particles, N, volume, V, and temperature, T) ensemble and evolve over time according to the Langevin equation of motion, given in Supporting Information, with an integration time step of 6 fs. This time step is the largest for which energy is well conserved in these systems. The coupling strength, τ_T, of the Langevin equation controls the magnitude of the friction and stochastic noise terms applied to each particle, which we utilize to approximate the dynamics of a solvated system without using explicit solvent molecules.[23] In simulations used to measure protein diffusion, τ_T is tuned to 0.7 ps, which leads to an average diffusivity of CG lysozyme molecules in vacuum that is consistent with lysozyme's experimental free solution diffusivity of $D_0 = 1.2 \times 10^{-6}$ cm^2/s.[24] In simulations used to measure protein partitioning, τ_T is set to 100 ps, which provides less dampening of the dynamics and, thus, accelerates the adsorption of protein onto the surface, without affecting the thermodynamics governing the equilibrium adsorption behavior. The Langevin equation also serves as a thermostat, maintaining the average system temperature at $T_{ref} = 300$ K.

Electrostatic interactions are represented by the "reaction field" potential[25] given in Supporting Information. In this modified Coulombic potential, the dielectric constant ϵ_r governs the electrostatic interaction between two particles separated by a distance r_{ij} less than a cutoff r_c, and a homogeneous charged environment with dielectric constant ϵ_{rf} is assumed for $r_{ij} > r_c$. In our simulations, the inner dielectric ϵ_r is tuned to represent qualitatively the screening of electrostatics by the solvent and co– and counter–ions, as discussed in the Results section. While this approach obviously cannot capture competition between ions and protein molecules for binding sites or polarization caused by reorientation of water dipoles, it does provide a simplified way to control the relative ionic strength. A large ϵ_r significantly screens charged interactions and reduces protein affinity for the adsorbent similarly to a high salt concentration, while a lower ϵ_r is representative of more favorable binding conditions at low salt concentration.

The cutoff for the reaction field potential, $r_c = 2.58$ nm, as well as the cutoffs for the neighbor list, $r_{list} = 2.53$ nm, and for Lennard-Jones (LJ) interactions, $r_{vdw} = 2.47$ nm, are approximately five times the average radius of the CG beads of the lysozyme protein model, $\sigma_{prot,avg}$ (the choice of $\sigma_{prot,avg}$ is discussed later). Trial MD simulations of the

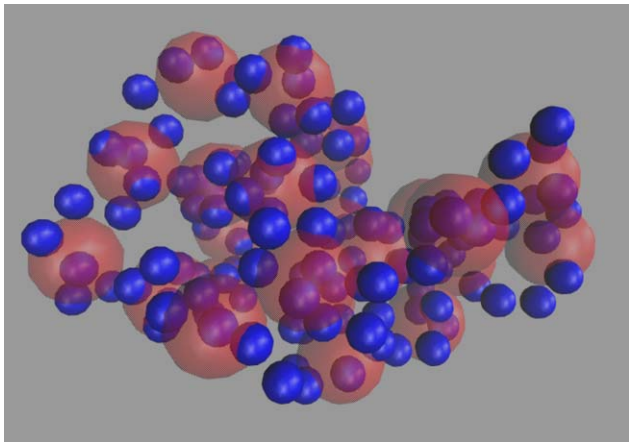

Figure 2. Mapping of C_α atoms of lysozyme (shown in blue) to CG model with $n_{CG}=5$ particles per residue (shown in red).

[Color figure can be viewed in the online issue, which is available at wileyonlinelibrary.com.]

macroporous system with different r_c values (with r_{list} and r_{vdw} scaled proportionally, $\epsilon_r=10$, and $N=210$ protein molecules) show that the radial distribution of protein molecules relative to the charged particles on the surface becomes invariant to the cutoff at $r_c \approx 5\sigma_{prot,avg}$, as seen in Figure S1 in Supporting Information.

Protein molecules

Each protein molecule is represented as a set of CG beads held together by a network of harmonic springs, with each bead representing multiple contiguous amino acid residues. The initial coordinates of each bead are found by averaging the positions of the α-carbon atoms of contiguous residues, as obtained from the lysozyme crystal structure (PDB code 1AKI).[26] The mass and charge of each bead are found by summing these quantities for the same residues.

Because the protein's charge distribution largely determines its interactions with the adsorbent, we determined an appropriate level of coarse graining that gives a charge distribution consistent with that of a fully atomistic model. We considered CG models with different integer numbers of residues per bead, n_{CG}, varying from 1 to 9, as described further in Supporting Information. Figure 2 shows an example mapping of each protein's C_α atom to the $n_{CG}=5$ model. For each different CG model, the electrostatic potential V_{CG} was evaluated at approximately 200 points on a rectangular lattice surrounding the protein molecule, and compared with the potential at the same points surrounding a fully atomistic model of the protein, V_{atom}. For lysozyme, models with $n_{CG}=6$ or higher exhibit a significant increase in the error of the linear fit to V_{CG} vs. V_{atom}, Therefore, the $n_{CG}=5$ model (with 25 total beads) is used in our production simulations. This model exhibited an R^2 value of greater than 0.99 for the linear fit to V_{CG} vs. V_{atom}.

To maintain the protein in the natively folded conformation, an elastic network model[27] is used to define harmonic bonds of the form $V_{bond}=\frac{1}{2}k_b(r_{ij}-b_{ij})^2$ between all CG particle pairs whose separation distance, r_{ij}, is 1.5 nm or less in the initial structure. The equilibrium bond length b_{ij} for a given pair is defined as r_{ij} in the native structure. The spring constant $k_b=1500$ kJ/mol is applied uniformly to all pairs. This value of k_b was found to give a root mean square deviation (RMSD) of the CG model's structure most consistent with the RMSD of the same virtual coordinates of the atomistic model, as discussed in Supporting Information.

The excluded volume of each CG bead is described by a purely repulsive LJ potential of the form $V_{LJ}=C_{12}/r_{ij}^{12}$, where $C_{12}=4\epsilon_i\sigma_i^{12}$ and σ_i and ϵ_i are the LJ radius and energy well depth, respectively, of bead i. The r^{-6} dispersion term of the standard LJ potential is neglected because including this term led to protein aggregation in preliminary simulations, an effect which is not observed experimentally for these systems. Therefore, this model assumes that protein–protein dispersion forces are canceled out by dispersion between proteins and the fictitious solvent, as well as other forces such as hydrophobic desolvation penalties.

As described in detail in Supporting Information, the parameters σ_i and ϵ_i for each CG bead depend on the σ and ϵ values of all non-hydrogen atoms in the residues that comprise the CG bead, obtained from the OPLS-AA force field.[28] For σ_i, the atomic σ values are used to determine the relative size of each bead, and then the beads are uniformly scaled such that the resulting CG model exhibits a radius of gyration of $R_g=1.36$ nm, consistent with the atomistic protein model. The σ_i values for the $n_{CG}=5$ model range from 0.70 to 0.83 nm. Each ϵ_i is defined as the sum of the ϵ values of all non-hydrogen atoms in the bead.

Functionalized pore surface

For both types of materials, the adsorbent pore is modeled as two parallel surfaces functionalized with charged groups, as shown in Figures 1a, b. Two surfaces are modeled rather than a single surface to create a homogeneous charged polymer phase that more closely approximates what would exist in a dextran-grafted macropore with a diameter consistent with experimental observations.[5] The idealized parallel surface model is used because while the physical agarose matrix is expected to have a highly heterogeneous pore structure based on transmission electron microscopy (TEM) images, we hypothesize that lysozyme's adsorption and diffusion behaviors will be roughly independent of the large-scale curvature of the pore surface. Each sulfonate group functionalized to the surface is represented by a single CG particle with a fixed location and a charge of -1. Because protein adsorption is dominated by electrostatics interaction with the charged groups in these systems,[7] the underlying agarose is modeled implicitly by repulsive walls defined at the bottom and top of the simulation box. The excluded volume of both this wall and the charged particles is given by the potential $V_{LJ}(r)=C_{12}/r^{12}$, where σ and ϵ are the same as the LJ parameters used for the dextran monomers discussed in the next section.

The spatial distribution and density of surface charged groups are not directly constrained by experimental data but are expected to affect surface adsorption and diffusion behaviors. We vary the positions of the charged groups relative to the bottom and top of the simulation box to partially model the expected heterogeneity of the underlying agarose structure. Any specific choice for these positions is somewhat arbitrary, as they are not constrained by experiment at the nanometer scale. Even a random structure requires choices for the distribution of heights of peaks relative to low points on the surface and the distribution of widths of these peaks. We therefore use a sinusoidal function to define the charged group positions, which allows us to systematically vary in a simple way just two length

scales (peak height and separation), and obtain near-negligible surface diffusion, as is observed experimentally. The vertical position of each charged group, z_i, is defined by the two-dimensional (2-D) sine wave $z_i = A_{\text{surf}} \sin(x_i/T_{\text{surf}}) \sin(y_i/T_{\text{surf}})$ with amplitude A_{surf} and period T_{surf}. The coordinates x_i, y_i are defined by a hexagonal packing arrangement, which maximizes the minimum lateral distance between neighboring charged groups for a given surface density of ligands. Without additional information such an arrangement is a reasonable choice, as during the functionalization process the charged ligands are likely to adopt a low energy configuration on the surface.

The density of charged groups on the surface, n_{SL}/S ("SL" denotes surface ligand) cannot be estimated directly from the experimental charge content of a macroporous adsorbent, because the physical charged groups functionalized to activated agarose monomers may not all be accessible to protein molecules. A series of multiscale simulations were used to determine appropriate values for A_{surf}, T_{surf}, and n_{SL}/S, as discussed in the Results section.

In both the macroporous and polymer-grafted systems, the pore surfaces have lateral dimensions of $x_{\text{pore}} = 40.2$ nm $\times$ $y_{\text{pore}} = 34.8$ nm. In the latter system with four polymer grafts per surface, these dimensions are consistent with the dextran content of the experimental material, as discussed below. The repulsive walls representing agarose are defined at the bottom and top of the simulation box ($z = 0$ and $z_{\text{box}} = 28$ nm, respectively) such that the nearest charged groups of the opposite surfaces are separated by a distance $z_{\text{pore}} = 21$ nm, which is consistent with the accessible pore radius, r_{pore}, of the physical macroporous agarose particles.[5]

Polymer grafts

In the polymer-grafted system, each charged dextran graft is represented by a coarse-grained model with one CG bead per dextran monomer. The 40 kDa dextran chains used in previous experiments are approximated by model chains composed of 250 beads.[5] The dextran side chain branches and sulfonate functional groups are modeled implicitly by assigning a charge of -1 to a fraction of the monomers, as discussed later. The polymer model is designed to exhibit a persistence length consistent with physical dextran and an excluded volume consistent with that of the lysozyme model. These criteria are satisfied by the 1 bead/monomer model, though more and possibly less detailed models could also meet the criteria.

The excluded volume of each monomer is described by a purely repulsive LJ potential, and protein molecules are attracted to the polymers solely through electrostatic interaction with the charged monomers. This model assumes that dispersion forces between the protein and the neutral polymer are canceled out by dispersion between proteins and the fictitious solvent. To ensure that the relative sizes of the polymer and protein are consistent, σ_{dextran} is calculated from the average radius of the protein's CG beads, $\sigma_{\text{prot,avg}}$, assuming that the mass m of each CG particle is proportional to its volume, such that $\sigma_{\text{dextran}} = (m_{\text{dextran}}/m_{\text{prot,avg}})^{1/3}(\sigma_{\text{prot,avg}})$. For the $n_{\text{CG}} = 5$ protein model this leads to $\sigma_{\text{dextran}} = 0.51$ nm. $\epsilon_{\text{dextran}}$ is estimated as the sum of the ϵ values of all non-hydrogen atoms in a dextran monomer.

Bonds between adjacent monomer are described by the finitely extensible nonlinear elastic potential, $V_{\text{bond}} = -\frac{1}{2} k_{\text{F}} b_{\text{F}}^2 \log\left(1 - \frac{r_{ij}^2}{b_{\text{F}}^2}\right)$, where b_{F} is the maximum allowed separation between a bonded pair and k_{F} is the spring constant. We define $b_{\text{F}} = 1.5\sigma_{\text{dextran}}$ and $k_{\text{F}} = 25 k_{\text{B}} T/\sigma_{\text{dextran}}$ (with k_{B} the Boltzmann constant and $T = 300$ K), as these conventions have been found previously to provide an appropriate amount of polymer stretching.[29] To assess the structural flexibility of the model dextran, we calculated the chain's persistence length, L_{p}, according to $\langle \cos\theta_{ij} \rangle = \exp(-(j-i)l/L_{\text{p}})$, where θ_{ij} is the angle between consecutive bonds i and j, and l is the distance between two monomers. A 250-membered neutral chain simulated in vacuum with Langevin dynamics exhibited $L_{\text{p}} = 0.61 \pm 0.04$ nm, which is within a range of experimental values reported for physical dextran of 0.4 nm[30] to 0.65 nm.[31]

Each chain is "grafted" to the surface by fixing the position of its first monomer at a location near the surface. The fixed monomers are distributed laterally in a hexagonal arrangement such that each is equidistant to its nearest neighbors, and each is placed at the height of the would-be nearest surface charged group, which is replaced by the monomer. Both surfaces are grafted with four polymer chains, which for the dimensions x_{pore} and y_{pore} given above corresponds to a graft density of 1 chain per 350 nm^2. This graph density is estimated from ρ_{dex}/S_v, where ρ_{dex} is the dextran content per adsorbent volume of the experimental material (18 mg/cm^3 for 40 kDa dextran grafts).[5] S_v is the pore surface area per adsorbent volume, estimated as $S_v = 2\epsilon_{\text{p}}/r_{\text{pore}}$, which assumes the adsorbent has a porosity ϵ_{p} and idealized cylindrical pores with a uniform pore radius r_{pore}. Values of $\epsilon_{\text{p}} = 0.9$ and $r_{\text{pore}} = 19$ nm are used in our calculations, consistent with the experimental data in Ref. 5.

The charge content per polymer graft, $n_{\text{L}}/n_{\text{poly}}$, is expected to greatly affect protein–polymer interaction. For the experimental system, the charge content is expected to be related to the degree of side-chain branching of the dextran used. The latter is expected to be on the order of 5% but can vary significantly.[32,33] Unfortunately, a directly determined value is not available for the experimental system considered in this work. There is also uncertainty associated with the fraction of primary hydroxyl groups on the chain termini that are functionalized. Thus, in this study, we simply assume 5% side chain branching and complete functionalization of all chain termini, such that $n_{\text{L}}/n_{\text{poly}} = 0.05$.

To measure the concentration of the free solution, C, in equilibrium with the polymer-grafted pore, we model a void volume adjacent to the pore, as seen in the MD snapshot shown in Figure 3. The polymer grafts are confined to the pore volume by two walls of purely repulsive particles whose positions are fixed at $y = 0$ and $y = y_{\text{pore}}$, the boundaries between the pore and the void volumes. These particles interact only with the polymers, allowing protein molecules to access both the pore and the void. The particles are arranged in a hexagonal close packing arrangement with a separation of 1 nm from their nearest neighbors, and have the same C_{12} parameter used for the agarose walls. Simulations of systems with different pore lengths ($y_{\text{pore}} = 34.8$ and 69.6 nm) exhibit time-averaged protein concentrations within the polymer phase that are statistically indistinguishable, indicating that any effects of the repulsive walls on the polymer phase structure do not affect protein affinity for this phase.

The void region has a length of $3y_{\text{pore}}$ such that the simulation box for the polymer-grafted system has lateral dimensions $x_{\text{box}} = 40.2$ nm $\times$ $y_{\text{box}} = 104.4$ nm. In the macroporous system, it is assumed that the concentration of protein in the

Figure 3. Snapshot from an equilibrated MD simulation of lysozyme in a polymer-grafted system.

The void region adjacent to the adsorbent provides a control volume in which the free solution concentration, *C*, in equilibrium with the adsorbed phase can be measured. [Color figure can be viewed in the online issue, which is available at wileyonlinelibrary.com.]

pore and not bound to the surface (referred to as the "pore space" in the remainder of this article) would be in direct equilibrium with the free solution. Thus, in these systems C is estimated within the pore space and the void region is not included, such that the simulation box has lateral dimensions $x_{box} = 40.2$ nm $\times$ $y_{box} = 34.8$ nm. Both systems have a box height of $z_{box} = 28.0$ nm, and periodic boundary conditions are applied in the x and y dimensions.

Determining equilibrium adsorption behavior

The equilibrium adsorption behavior is determined by running MD simulations of the adsorbent pore with various protein loadings, N, and measuring the local protein concentrations in different regions of the pore at equilibrium. Although equilibrium concentrations could be measured using semigrand canonical MD simulation in which the total number of particles is constrained and the number in each region fluctuates, this ensemble is not currently supported in the GROMACS code used for this work, and the nonstandard molecular models used here are not implemented in the codes that do support this ensemble.

Each simulation of a particular adsorbent type, electrostatic strength, and protein loading is initialized by incrementally inserting protein molecules into the simulation box at random locations and orientations, followed by steepest descent energy minimization. The majority of molecules are initialized in the interior region of the pore, such that they to not interact with the charged surface. Following energy minimization, the system is equilibrated in the NVT ensemble with $\tau_T = 100$ ps used to accelerate the dynamics, and thus enhance the equilibration process. The simulation time is sufficiently long for the free solution protein concentration to reach equilibrium with the surface and polymer regions, as discussed later.

Three different local concentrations are measured, corresponding to the three distinct types of protein adsorption behaviors that are observed in the MD simulations. A protein molecule whose center of mass is within a distance $r_{surf} = 3$ nm of a surface charged group is considered to be surface bound at a given time. This value of r_{surf} was determined by considering the distribution of distances between a protein molecule and the nearest surface charged group at equilibrium, as shown in Figure S4 of Supporting Information. For all tested electrostatic strengths, $r_{surf} = 3$ nm encompasses the peak in the distribution at short separations corresponding to surface-bound protein, and excludes molecules not bound to the surface with longer separations. The concentration of surface-bound protein on a particle volume basis, q_s, is calculated as

$$q_s = \frac{\langle N_s \rangle}{S} m_{prot} S_v \tag{2}$$

where $\langle N_s \rangle / S$ is the time-averaged number of surface-bound protein molecules per unit surface area and m_{prot} is the protein molecular mass. The surface area over which N_s is measured is defined at a distance of $\Delta y = 8$ nm away from the ends of the adsorbent in the y dimension, to avoid unintended effects of the repulsive walls of the polymer-grafted system on surface adsorption.

A second type of molecular behavior is that of protein molecules within the pore space and not bound to the surface. The concentration of these molecules is defined as

$$c_p = \frac{\langle N_p \rangle}{S} m_{prot} S_v \tag{3}$$

where $\langle N_p \rangle$ is 1/2 the time-averaged number of protein molecules within the pore space at a distance of $r_{surf} = 3$ nm or more from the nearest surface charged group. The factor of 1/2 is used because like q_s, c_p is predicted based on the number of protein molecules per unit surface area S, and the top and bottom planes of the system are considered separate surfaces. For the polymer-grafted system, $\langle N_p \rangle$ includes protein molecules that interact directly with the polymer charged groups as well as those that do not interact. In both systems, the total concentration of protein in the adsorbent includes protein molecules on the surface as well as those in the pore space, and is defined as $\hat{q} = q_s + c_p$.

Finally, a third type of behavior is that of protein molecules in the simulated free solution or in equilibrium with a hypothetical free solution, whose concentration is calculated as

$$C = \frac{\langle N_{free} \rangle m_{prot}}{V_{free}} \tag{4}$$

where $\langle N_{free} \rangle$ is the time-averaged number of molecules in a volume V_{free} where proteins are unaffected by surface charged groups or repulsive walls. In the macroporous system, V_{free} is defined in the pore space at a distance $\Delta z = 8$ nm from $z = 0$ and $z = z_{box}$ to avoid the effects of the charged surfaces. In the polymer-grafted system, V_{free} is defined in the void region adjacent to the adsorbent, at a distance $\Delta z = 8$ nm from $z = 0$ and $z = z_{box}$, and at a distance $\Delta y = 8$ nm from $y = y_{pore}$ and $y = y_{box}$, to avoid possible effects of the purely repulsive walls at the ends of the pore.

The equilibrium value of each local concentration is determined by averaging its time series over a period of 480 ns or longer over which C exhibits stable oscillations about its mean. The time required to reach this equilibrium varies from 200 to 2000 ns, and generally is longer for systems with grafted polymers, high protein loadings, and low ϵ_r. The standard error in the mean for each concentration is calculated as $\sigma / \sqrt{(n_e - 1)}$, where σ is the standard deviation of the equilibrated portion of the time series and n_e is number of uncorrelated samples in that region. $n_e = n/(2\tau_{ACF})$, where n is the original number of samples and τ_{ACF} is the decay constant of an exponential function fit to the autocorrelation function of the time series of concentration C after equilibration.

Determining molecular diffusivities

Average molecular diffusivities of protein adsorbed to the surface, D_s, and within the pore space (either open or polymer filled), D_p, are determined for each type of adsorbent and electrostatic strength. The diffusivities are measured from an MD simulation with a coupling strength $\tau_T = 0.7$ ps and a protein loading N that leads to $C = 1-3$ mg/cm^3 at equilibrium, that is, a nearly saturated adsorbed phase.

The diffusivity of a protein molecule over a given time window is determined from the slope of its N_{dim}–dimensional mean squared displacement (MSD) according to the Einstein relation

$$2\tau D = \frac{1}{N_{dim}} \langle |r_i(t+\tau) - r_i(t)|^2 \rangle \tag{5}$$

where τ is the offset time, the braces denote averaging over multiple reference times t, and r_i is the molecule's center of mass coordinate. Our MD simulations show that protein molecules not adsorbed to the surface, either in an open macropore or within the polymer-filled pore space, exhibit isotropic diffusion, while molecules on the surface are restricted to the xy plane. Therefore, 3-D and 2-D MSD curves are used to evaluate the diffusivities of molecules with these respective adsorption behaviors.

Whether or not a protein molecule is surface adsorbed also determines the length of the trajectory used to calculate the MSD, Δt_{msd}, and the region of the MSD over which D is estimated, as discussed in the Results section. The ensemble-averaged D_s and D_p are determined by averaging the MSD curves of all molecules that remain in the same adsorption state (i.e., on or off of the surface) for the entire period Δt_{msd}, and evaluating the slope of the ensemble-averaged MSD. Only including molecules that remain in the same adsorption state for the entire Δt_{msd} avoids bias from rare events in which a molecule desorbs or readsorbs to the surface. The standard error of the mean of D_s and D_p is estimated by bootstrapping with 50 bootstrap repetitions.

Predicting adsorption kinetics

Numerical simulations of diffusional mass transfer are used to predict the effective protein transport rate as a function of properties that cannot be directly measured by experiment, including the diffusivities of protein molecules in distinct regions of the pore and the partitioning of protein between those regions. The following conservation equation and initial and boundary conditions describe transient adsorption into a spherical particle of radius R over time t and radial distance r

$$\frac{\partial c_p}{\partial t} + \frac{\partial q_s}{\partial t} = \frac{1}{r^2}\frac{\partial}{\partial r}\left[r^2\left(D_p\frac{\partial c_p}{\partial r} + D_s\frac{\partial q_s}{\partial r}\right)\right] \tag{6a}$$

$$q_s = f(c_p) \tag{6b}$$

$$r = 0 : \frac{\partial c_p}{\partial r} = 0 \tag{6c}$$

$$r = R : c_p = f(C_0) \tag{6d}$$

$$t = 0 : c_p = q_s = 0 \tag{6e}$$

where $f(c_p)$ describes the local equilibrium between protein on the surface and in the pore space, that is, the q_s vs. c_p adsorption isotherm. As discussed in the Results section, for each system this isotherm is well described by the Langmuir model given in Eq. 9 with parameters $q_{m,s}$, the saturation capacity of the surface (defined on an adsorbent volume basis), and K_s, the equilibrium constant for protein adsorption from the pore space onto the surface (defined on a free solution volume basis). C_0 is the protein concentration of the extra-particle bulk solution, assumed to be constant at 2.0 mg/cm^3. The boundary condition $c_p = f(C_0)$ at $r = R$ is determined from the local equilibrium between protein in the bulk and in the pore space, that is, the c_p vs. C isotherm. As described in the Results, in the polymer-grafted systems this local equilibria is described by the Langmuir model given in Eq. 10, with a saturation capacity $c_{p,m}$ and equilibrium constant K_p. In the macroporous system, the bulk-pore space equilibria is described by $c_p = K_D C$ (Eq. 11). The isotherm parameters as well as D_p and D_s are determined from MD simulation.

The numerical simulations are performed by expressing Eq. 6 in terms of c_p based on the q_s-c_p local equilibria, and solving by the method of lines.[34] The particle-averaged protein concentration at a given time is then calculated as

$$\bar{q} = \frac{3}{R^3}\int_0^R r^2 \hat{q}(r) dr \tag{7}$$

where $\hat{q}(r)$ is the total protein concentration at position r within the simulated particle, and includes molecules both on and off of the surface.

To quantify the adsorption rate predicted by a simulation, following the procedure of Stone and Carta, we define an apparent effective pore diffusivity, $D_{e,app}$, as the pore diffusivity that would give the same adsorption kinetics as that obtained experimentally for a macroporous matrix with a rectangular adsorption isotherm and conditions where $q_s \gg c_p$.[5] In this case, the batch uptake curve ($\bar{q}$ vs. t) is given by the following equation

$$\frac{1}{2} - \frac{1}{3}\frac{\bar{q}}{\hat{q}^*} - \frac{1}{2}\left(1 - \frac{\bar{q}}{\hat{q}^*}\right)^{\frac{2}{3}} = \frac{C_0}{\hat{q}^*}\frac{D_{e,app}t}{r_p^2} \tag{8}$$

where $\hat{q}^*$ is the protein concentration in the adsorbent particles at equilibrium. $D_{e,app}$ is estimated by fitting the simulated batch uptake curve with Eq. 8, by minimizing the squared error between the fitted curve and the data over the region from $t = 0$ to the time at which $\bar{q} = \hat{q}^*$.

Results

Effects of protein diffusion and partitioning on macroscopic adsorption kinetics

A series of mass transfer simulations based on Eq. 6 were performed to study the relationships between molecular-level properties and the effective transport rate, which helps guide the parameterization of molecular model details that are not directly constrained by experimental data. The molecular-level properties of interest include the protein diffusivities D_s and D_p, the favorability of protein adsorption from the pore space (which may or may not include polymer) onto the surface, quantified by K_s, the saturation capacity of the surface, $q_{m,s}$, and for the polymer-grafted system, the Langmuir isotherm parameters K_p and $c_{p,m}$ for partitioning from the bulk into the polymer-filled pore space. In these systems, the affinity of protein for the charged polymers impacts both the partitioning between the surface and the pore space, and between the pore space and the bulk, through the parameters K_s and K_p, respectively. The partitioning between the polymer-filled pore space and the bulk only affects the

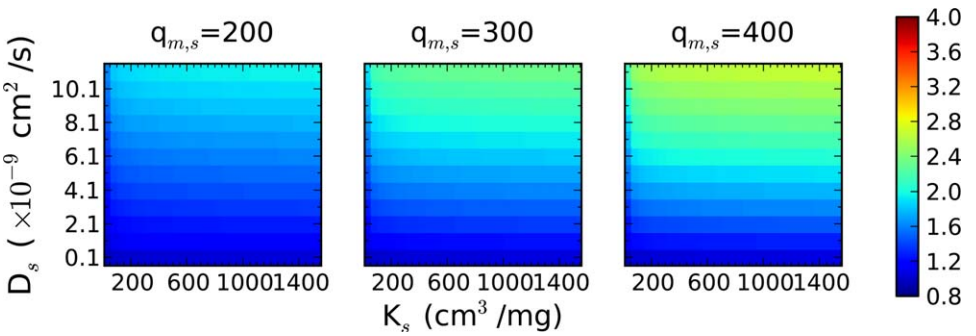

Figure 4. Predicted $D_{e,app}/D_0$ for lysozyme in a macroporous system based on numerical simulation of mass transfer with different values of D_s, K_s, and $q_{m,s}$ (units of mg/cm^3), assuming $D_p=D_0$ and $c_p|_{r=R}=C_0$ for protein molecules in an open macropore.

According to this model, the effective transport rate increases primarily with the diffusivity of surface-bound protein D_s, as shown in the upper regions of each plot, although the surface capacity $q_{m,s}$ and favorability of adsorption to the surface K_s have some effect on the effective transport rate. [Color figure can be viewed in the online issue, which is available at wileyonlinelibrary.com.]

solution of Eq. 6 through the value of $c_p(C=C_0)|_{r=R}$, that is, the concentration of protein in the pore space at the edge of the particle that is in equilibrium with a bulk of constant concentration C_0. We thus use this as our independent variable rather than varying K_p and $c_{p,m}$ individually. For all molecular-level properties, the parameter ranges tested are representative of the protein behaviors observed in trial MD simulations. The overall transport rate is quantified by the $D_{e,app}$ fit to the simulated batch uptake curve.

Figure 4 shows how the transport of lysozyme in a macroporous system depends on the diffusion and adsorption of protein on the surface as predicted by this model. The predicted $D_{e,app}/D_0$ is plotted as a function of K_s on the x axis, D_s on the y axis, and $q_{m,s}$ in the different subplots. In these simulations $D_p=D_0$, which assumes molecules in the open pore space diffuse as they would in free solution, and $c_p|_{r=R}=2.0$ mg/cm^3, which assumes the pore space concentration at the particle edge has the same concentration as the bulk.

In general, the transport rate is most dependent on the surface diffusivity D_s, although it has some dependence on the surface's saturation capacity $q_{m,s}$ and on the favorability of surface adsorption K_s, as well. For instance, at $q_{m,s}=400$ mg/cm^3, an increase in D_s of approximately two orders of magnitude raises $D_{e,app}/D_0$ by approximately one order of magnitude, while a two order of magnitude increase in K_s raises $D_{e,app}/D_0$ by only 10 to 25%. Additionally, the effect of K_s on $D_{e,app}/D_0$ depends only slightly on D_s. $D_{e,app}/D_0$ is also somewhat dependent on $q_{m,s}$, increasing by up to 35% when $q_{m,s}$ is doubled. The effective transport rate is most consistent with that predicted by ordinary pore diffusion (at which $D_{e,app}/D_0\approx 1$) when D_s is 1×10^{-9} cm^2/s or lower, for all K_s and $q_{m,s}$ values tested.

Figure 5 shows that in the polymer-grafted system, faster transport is predicted as protein partitioning from the bulk into the pore space increases, and as the diffusion of protein within the pore space increases. Each subplot shows $D_{e,app}/D_0$ as a function of K_s and D_p on the x and y axes, respectively. $q_{m,s}$ increases in the subplots from left to right, $c_p|_{r=R}$ increases from bottom to top, and D_s is kept constant at 0.5×10^{-9}cm^2/s, representing slow surface diffusion under strong binding conditions. $D_{e,app}/D_0$ is approximately a linear function of both $c_p|_{r=R}$ and D_p for fixed values of K_s and $q_{m,s}$ over the tested variable space. The transport rate is approximately independent of K_s and $q_{m,s}$ under these conditions, increasing by only 5% when K_s is increased from 2 to 1000 cm^3/mg (not shown). Figure S5 of Supporting Information shows $D_{e,app}/D_0$ predicted for different D_s and with $c_p|_{r=R}=20.0$ mg/cm^3, which shows that surface diffusion has a small effect on the overall transport rate in the polymer-grafted system compared to the macroporous system, as transport in the polymer-grafted adsorbent under favorable binding is dominated by the flux through the polymer-filled pore space.

These simulations can be used to constrain parameter values for molecular model details that are not directly obtainable from experimental data. For example, Figure 4 provides an upper bound on the surface diffusivity D_s that the model surface can allow if the overall transport rate is consistent with that predicted by ordinary pore diffusion, the dominant mass transfer mechanism in a macroporous material. Figure 5 provides lower bounds on the protein concentration within the polymer-filled pore space and the protein diffusivity D_p in this region if the enhancement in the transport rate is consistent with that observed in the experimental dextran-grafted material.

Effects of molecular model parameters on protein diffusion and partitioning

Table 1 lists molecular model parameters that lead to protein partitioning and diffusivities that are consistent with the experimental adsorption kinetics. These values are determined through a series of MD simulations of both adsorbent systems, as described in Supporting Information. The estimated standard error in the mean of each property is given in parenthesis. As shown, an inner dielectric constant of $\epsilon_r=10$ and a polymer charge content of $n_{SL}/S=0.05$ lead to levels of protein partitioning and diffusion within the polymer-filled pore space that correspond to an effective transport rate of $D_{e,app}/D_0=6.1\pm0.6$, in qualitative agreement with experimental results for dextran-grafted systems at low ionic strength. In the macroporous system with $\epsilon_r=10$, a surface model with a charge density of 49 ligands/100 nm^2 and sine wave parameters of $A_{surf}=1/3d_{prot}$ and $T_{surf}=d_{prot}$ lead to levels of protein partitioning and diffusion on the surface that correspond to $D_{e,app}/D_0=1.3\pm0.1$, which approaches the $D_{e,app}/D_0=1$ result expected for ordinary pore diffusion. Therefore, the production MD simulations of this study are performed with the adsorbent model parameters given above and with $\epsilon_r=10$ used to represent favorable binding conditions.

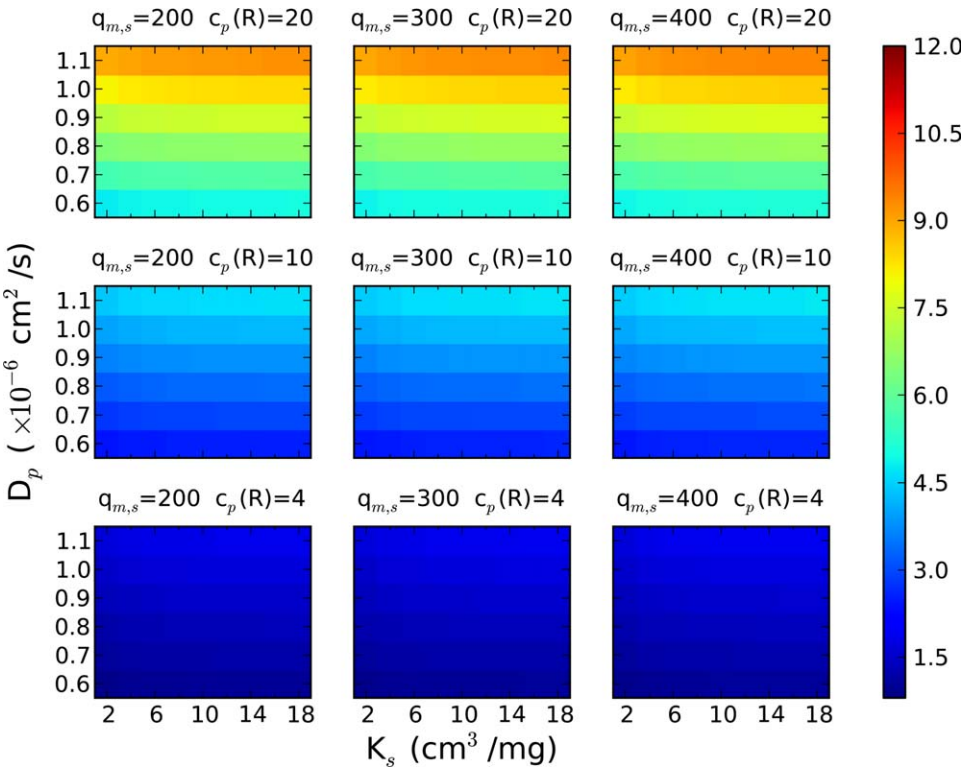

Figure 5. Predicted $D_{e,app}/D_0$ for lysozyme in a polymer-grafted system based on numerical simulation of mass transfer with different values of D_p, K_s, $q_{m,s}$ (units of mg/cm^3), and $c_p|_{r=R}$ (representing different levels of partitioning into the pore), with $D_s=0.5\times10^{-9}$cm^2/s.

According to this model, the effective transport rate is most enhanced when protein partitioning from the bulk into the pore is favorable, as seen in the upper subplots, and when diffusion in the polymer-filled pore is fast, as seen in the upper third of each subplot. [Color figure can be viewed in the online issue, which is available at wileyonlinelibrary.com.]

Comparable transport rates can also be obtained using alternate parameters for the surface geometry. However, such geometries can affect the adsorption and diffusion behaviors of protein on the surface. The model with $A_{surf}=1/3d_{prot}$ exhibits a single type of adsorption site, while a model with $A_{surf}=2/3$ d_{prot} (i.e., larger peaks and troughs) and the same T_{surf} and n_{SL}/S exhibits two types of adsorption sites, as shown in plots of the protein number density with respect to z position in the pore, plotted in Figure S6 of Supporting Information. The former (shallower peaks) leads to a relatively uniform distribution of surface diffusivities of individual protein molecules. However, the latter model with higher amplitude leads to rare events in which protein molecules diffuse up to an order of magnitude faster than the ensemble average of D_s. These fast-diffusing molecules generally interact with a single charged group located at high z positions on the surface, while the majority of adsorbed molecules interact with multiple charged groups at lower positions. In this work, we use a molecular model that provides a more uniform distribution of surface diffusivities to be consistent with the macroscopic transport model that assumes a single average diffusion constant on the surface. The effects of surface heterogeneity on the heterogeneity of protein dynamics is a subject to be explored in later research.

Table S2 in Supporting Information describes the effect of the surface geometry parameters on D_s. MD simulations were conducted with various surface geometries, including a completely smooth surface in which the charged groups have a uniform height, and heterogeneous structures with different values of A_{surf} and T_{surf}. The resulting D_s values (with $\epsilon_r=12$) vary from 1×10^{-8} to 1×10^{-7} cm^2/s, with the fastest diffusivities generally observed when $T < d_{prot}$, as protein molecules cannot access the troughs of the surface. The smooth surface also leads to $D_s=1.7\times10^{-7}$ cm^2/s for $\epsilon_r=12$. These results as well as the predicted $D_{e,app}/D_0$ vs. D_s relationships shown in Figure 4 demonstrate that some inhomogeneity in the surface structure is necessary to obtain a transport rate consistent with the pore diffusion mass transfer mechanism.

Table 1. Summary of Molecular Model Parameters (MD Inputs), Resulting Protein Diffusivities and Adsorption Isotherm Parameters (MD Outputs), and the Effective Transport Rates Predicted Using MD Outputs

Model detail (MD Inputs)	Macroporous	Polymer-grafted
ϵ_r	10	10
n_L/n_{poly}	n/a	0.05
n_{SL}/S (ligands/100 nm^2)	49	49
A_{surf}	$1/3d_{prot}$	$1/3d_{prot}$
T_{surf}	d_{prot}	d_{prot}
Molecular behavior (MD outputs)	**Macroporous**	**Polymer-grafted**
D_s ($\times10^{-9}$ cm^2/s)	1.3 (0.2)	0.6 (0.4)
D_p ($\times10^{-6}$ cm^2/s)	1.2 (0.1)	0.8 (0.1)
$q_{m,s}$ (mg/cm^3)	262 (<1)	249 (<1)
K_s (cm^3/mg)	64 (7)	11 (3)
$c_p(r=R)$ (mg/cm^3)	2.1 (<1)	17.9 (0.3)
Transport rate	**Macroporous**	**Polymer-grafted**
$D_{e,app}/D_0$	1.3 (0.1)	6.1 (0.5)

Numbers in parenthesis give the standard error of the mean.

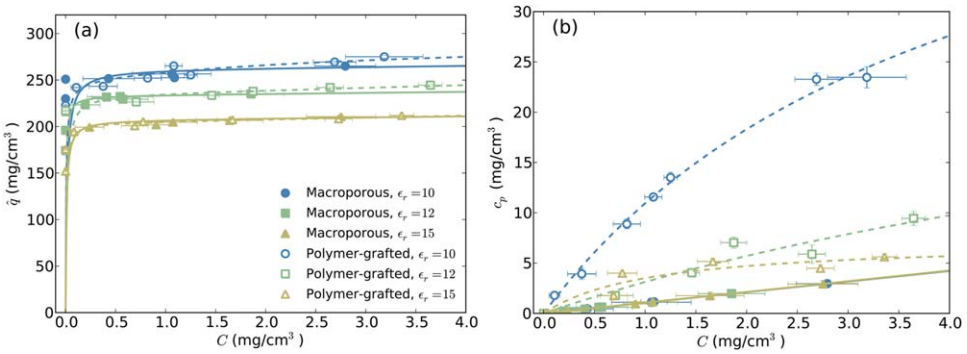

Figure 6. Adsorption isotherms predicted by MD simulation for (a) $\hat{q}$ vs. C and (b) c_p vs. C.

The isotherms given in (a) show that when electrostatic interactions are weaker (at high ϵ_r values), the overall adsorption capacity decreases for both the macroporous (filled symbols) and the polymer-grafted (open symbols) systems. Protein partitioning into the polymer-filled pore also decreases as electrostatics become weaker, as shown in (b). Error bars show the standard error of the mean concentrations. [Color figure can be viewed in the online issue, which is available at wileyonlinelibrary.com.]

Equilibrium adsorption behavior

MD simulations were performed using the adsorbent model parameters discussed above and different ϵ_r values to study how the strength of electrostatics affects the adsorption equilibria predicted by the model. Figure 6a shows simulated adsorption isotherms of $\hat{q}$ vs. C for both types of adsorbents, with ϵ_r values of 10, 12, and 15 representing low, moderate, and high ionic strengths, respectively. Each isotherm is fit with $\hat{q}=q_s+c_p$, based on the fitted q_s vs. c_p and c_p vs. C isotherm models described below. As shown, both adsorbents exhibit a lower adsorption capacity when electrostatic interactions are weaker, which is qualitatively consistent with experiments showing reduced lysozyme adsorption at high salt concentrations.[7] The adsorbents also become saturated at solution concentrations of $C=1$ to 3 mg/cm^3, which is consistent with the experimental saturation concentrations.

The simulations do not predict an enhancement in the overall adsorption capacity of the polymer-grafted system vs. the macroporous when electrostatics are strong. However, experiments conducted at low ionic strength found the capacity was only approximately 10 to 20% higher in dextran-grafted particles than in macroporous particles with a similar backbone and a slightly (6% higher) total charge content.[7] Given the resolution of the model, this relatively small discrepancy is likely not a concern.

Nevertheless, the slightly lower than expected capacity of the polymer-grafted system can be understood by considering the local equilibria between q_s and c_p and between c_p and C. Figure S7 in Supporting Information shows q_s vs. c_p isotherms, which generally are very favorable and, therefore, are fit with the following Langmuir model:

$$q_s=\frac{q_{m,s}K_s c_p}{1+K_s c_p} \tag{9}$$

The macroporous system exhibits a higher surface capacity than the polymer-grafted case when electrostatics are strong and approximately the same surface capacity when electrostatics are weaker, as seen in the isotherms and in the fitted $q_{m,s}$ values reported in Table 2, because the polymer grafts occupy a non-negligible area on the surface and thus reduce the effective number of surface binding sites.

Figure 6b provides the c_p vs. C isotherms, which show that the charged polymers can enhance protein partitioning from the bulk into the pore space when electrostatics are strong. However, this enhancement is negated by the reduction in surface adsorption due to the grafts, resulting in very similar total capacities for the two adsorbents. At high ϵ_r, the protein shows little preference for the polymer-filled pore over the bulk. The fact that even with strong electrostatics, adsorption to the polymers is sufficiently low that it is negated by the reduced surface adsorption, whereas experiments show an overall enhancement due to the polymers, suggests that the actual dextran charge content may be greater than 5%, that the actual protein may have a greater effective charge, that nonelectrostatic forces might contribute moderately to protein–polymer binding, or some combination of all three. The c_p vs. C isotherms are fit with the Langmuir model shown in Eq. 10 for the polymer-grafted systems, and with the linear model shown in Eq. 11 for the macroporous systems:

$$c_p=\frac{c_{p,m}K_p C}{1+K_p C} \tag{10}$$

$$c_p=K_D C \tag{11}$$

Table 2. Summary of Fitted Isotherm Parameters

System	ϵ_r	$q_{m,s}$ (mg/cm^3)	K_s (cm^3/mg)	$c_{p,m}$ (mg/cm^3)	K_p (cm^3/mg)	K_D
Macroporous	10	262 (<1)	64 (7)	–	–	1.06 (0.05)
Macroporous	12	233 (<1)	217 (46)	–	–	1.06 (0.10)
Macroporous	15	207 (<1)	107 (14)	–	–	1.06 (0.07)
Polymer-grafted	10	249 (<1)	11 (3)	51 (3)	0.27 (0.03)	–
Polymer-grafted	12	235 (<1)	31 (2)	33 (37)	0.10 (0.05)	–
Polymer-grafted	15	204 (<1)	80 (14)	7 (<1)	0.96 (0.13)	–

Protein partitioning onto the surface and into a polymer-filled pore is greatest at $\epsilon_r=10$, at which electrostatics are strong. Adsorption isotherms measured from MD simulation are quantified by fitting data with either a langmuir or linear isotherm model. Dashes denote parameters with very large error estimates due to the poor fit of the specified model. Numbers in parenthesis give the standard error of the mean.

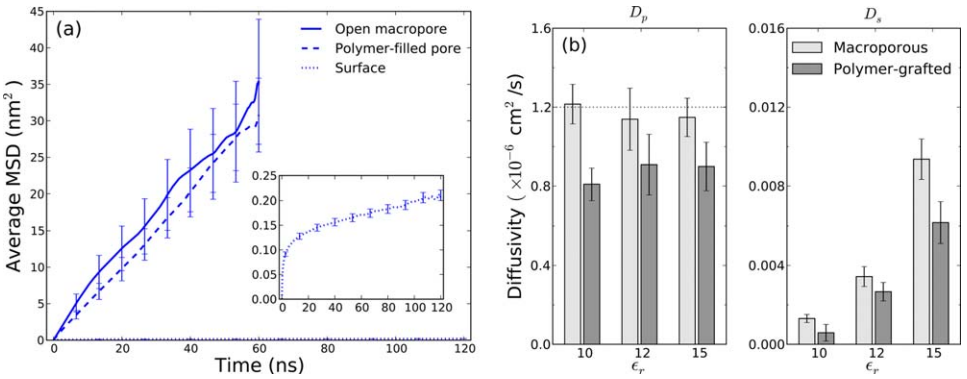

Figure 7. MD simulations show that the molecular diffusion of lysozyme depends on the location of the protein within the pore and on the strength of electrostatics.

(a) Average MSDs of protein molecules in different phases within a pore, for favorable binding conditions represented by $\epsilon_r = 10$. (b) Average diffusivity of protein in the pore space, D_p, and bound to the surface, D_s, for both adsorbent types and different ϵ_r values. The experimental free solution diffusivity of lysozyme, D_0, is shown by the dotted line alongside the D_p results. Diffusion in the polymer-filled pore is up to 33% slower than in free solution, while diffusion on the surface is up to three orders of magnitude slower than D_0. Error bars show the standard error of the mean MSDs (a) and diffusivities (b). [Color figure can be viewed in the online issue, which is available at wileyonlinelibrary.com.]

For macroporous systems, K_D describes the equilibrium partitioning between the fictitious bulk solution and the open macropore. Slight deviations from a slope of $K_D = 1$ result from the different control volumes used to calculate c_p and C, as the former includes all molecules not bound to the charged surface, and the latter includes molecules that do not interact with the surface at all.

The isotherm models are fit to the c_p vs. C and q_s vs. c_p data by nonlinear regression, and uncertainties in the fitted parameters are estimated using a block bootstrap procedure. For each of 1000 bootstrap repetitions, an isotherm is constructed by evaluating the mean of concatenated, uncorrelated blocks of the original concentration time series for each protein loading used in the original isotherm. The block length is chosen as twice the decorrelation time of the instantaneous concentration. Each of these 1000 isotherms is fit with the appropriate model. The standard error in the mean of a given model parameter is estimated from the standard deviation of the 1000 predicted parameters.

Table 2 summarizes the fitted isotherm model parameters. The $q_{m,s}$ and $c_{p,m}$ values for the polymer-grafted systems show that the protein binds primarily to the surface, due to the greater number of multivalent interactions that can be made there. A surface-bound protein molecule interacts with approximately five charged groups on average, providing a very favorable enthalpy which outweighs the entropic penalty of losing translational degrees of freedom upon binding to the surface. A molecule associated with the charged polymers retains its translational motion but interacts with only 1–2 charged groups, making partitioning into this part of the pore less favorable. Finally, we note that although the near rectangularity of the q_s vs. c_p isotherm results in significant uncertainty in the initial slope (and thus K_s), the transport rates predicted from numerical simulation based on the parameters given in Table 2 are virtually unaffected by changes in K_s in this range.

Molecular diffusivities

MD simulations show that the diffusional mobility of a protein molecule depends on its location within the adsorbent and, if the molecule is adsorbed, on the strength of electrostatics. Figure 7a compares the ensemble-averaged MSD curves for protein within the pore space of the macroporous system, within the polymer-filled pore space, and adsorbed on the surface in the macroporous system, for $\epsilon_r = 10$ at which electrostatic interactions are strong. As shown, molecules not bound to the surface exhibit random walk behavior even at short time scales. In this case, individual D measurements are estimated from the slope of the curve between $t =$ 5 and 10 ns, using a 3-D MSD calculated from a 60 ns section of the trajectory. Molecules bound to the surface exhibit anomalous diffusion over short time scales and true random walk behavior only at longer times. In this case, individual D measurements are estimated from the slope of the curve between $t = 30$ and 60 ns, using an 2-D MSD calculated from a 120 ns section of the trajectory. These times are within the linear regions of the respective curves and avoid poor sampling at long times.

Figure 7b compares the ensemble-averaged diffusivities of protein in the pore space, D_p, and on the surface, D_s, for both adsorbents and different ϵ_r values. In the macroporous system, D_p is consistent with the experimental free solution diffusivity of $D_0 = 1.2 \times 10^{-6}$ cm^2/s (shown in the dotted line) and does not vary with ϵ_r, within error, as protein molecules in the open pore space do not interact with any charged groups. In the polymer-grafted system, D_p is within 30–40% of D_0. The effect of the charged polymers on the protein's diffusional mobility becomes more significant at $\epsilon_r = 10$. With $\epsilon_r = 8$ in a comparable polymer-grafted system (not shown), D_p is reduced to approximately 50% of D_0. D_p within the polymer-filled pore is independent of the local protein concentration in the pore space, as shown in Table S3 in Supporting Information, suggesting that protein–protein interactions do not impact the mobility under these conditions.

The observed D_s values are lower than D_0 by up to three orders of magnitude as a result of strong binding to the surface. In general, D_s increases as a function of ϵ_r, as the weaker adsorption when electrostatics are significantly screened enhances the mobility on the surface. The lower D_s values observed in the polymer-grafted system are attributed to the additional diffusional hindrance of the polymers grafted to the surface.

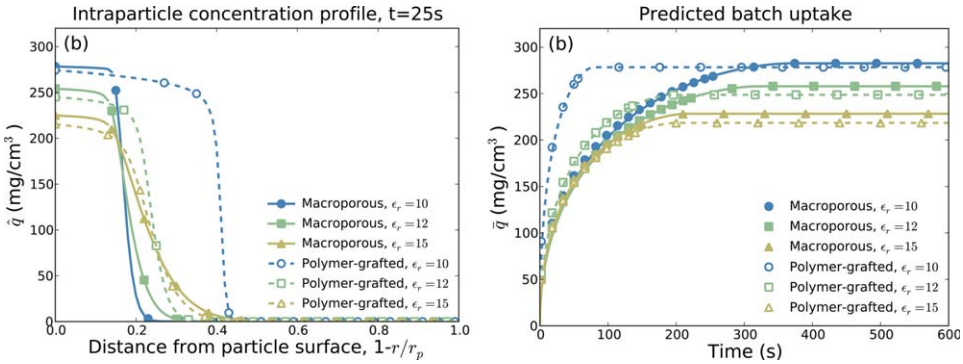

Figure 8. Mass transfer simulations show that when electrostatics are strong at ϵ_r=10, the polymer-grafted system provides faster adsorption kinetics than the macroporous, and when electrostatics are weak at ϵ_r=15, the two adsorbents exhibit comparable kinetics, as shown in (a) intraparticle profiles of the total protein concentration, $\hat{q}$, at t = 25 s and (b) batch uptake curves of the particle-averaged concentration, $\bar{q}$, vs. t.

[Color figure can be viewed in the online issue, which is available at wileyonlinelibrary.com.]

Adsorption kinetics

Numerical simulations based on the MD results given above are used to study how the strength of electrostatics affects the macroscopic adsorption kinetics. Figure 8a shows simulated intraparticle profiles of the total protein concentration in the adsorbent, $\hat{q}$, for the macroporous (filled symbols) and polymer-grafted (open symbols) systems for different ϵ_r. Under favorable binding conditions the polymer-grafted system exhibits faster adsorption kinetics than the macroporous, as seen in the fronts that evolve faster for ϵ_r=10 and 12. No enhancement is observed for ϵ_r=15. Both materials exhibit a sharp adsorption front at ϵ_r=10 and a more diffuse front as ϵ_r increases. This is due to the fact that surface adsorption becomes less favorable as electrostatics are more significantly screened. The shape of these curves compare qualitatively with infrared microscopy images of lysozyme adsorption in macroporous and dextran-grafted particles.[7]

Figure 8b plots batch uptake curves showing the particle-averaged concentration, $\bar{q}$, vs. time. The faster kinetics of the polymer-grafted system at low ϵ_r are evident in the shorter times required to reach saturation. In general, the time scales over which both adsorbents are predicted to saturate are comparable to those observed for the experimental systems, shown in Figure 1 of Ref. 7.

Figure 9a shows $D_{e,app}/D_0$ as a function of ϵ_r for both systems, determined by fitting the batch uptake curves of Figure 8b. For comparison, Figure 9b provides experimental $D_{e,app}/D_0$ values for lysozyme in physical macroporous and dextran-grafted systems at different ionic strengths, originally presented in Figure 2 of Ref. 7, and obtained using the same fitting procedure on the experimental batch uptake curves. Uncertainties in the simulated $D_{e,app}/D_0$ values are obtained by a bootstrap procedure with 50 bootstrap repetitions. For each repetition, $D_{e,app}/D_0$ is estimated using randomly selected isotherm parameters and diffusivities from the distributions of bootstraps samples, generated as discussed in the previous sections. The uncertainty in $D_{e,app}/D_0$ is estimated as the standard deviation of these 50 $D_{e,app}/D_0$ values.

The trends of the simulations and experiments are in qualitative agreement. Both show that $D_{e,app}/D_0$ is enhanced in the polymer-grafted system when electrostatics are strong, that is, low ϵ_r in the simulations and low salt concentration in the experiments, and that the polymer-grafted transport rate approaches that of the macroporous system as electrostatics become weaker. In both cases, $D_{e,app}/D_0$ in the macroporous system increases with respect to ϵ_r, which according to our modeling reflects the increase in surface diffusion as electrostatics become weaker.

Even for the strong-binding case of ϵ_r=10, surface diffusion has a non-negligible contribution to the overall transport rate, as seen in the result of $D_{e,app}/D_0 > 1$. The fact that the experiment shows $D_{e,app}/D_0 < 1$ under strong binding conditions indicates that our model surface deviates somewhat from the physical system. While trial MD simulations did not identify surface model parameters which led to $D_{e,app}/D_0 \to 1$, the numerical simulation results given in Figure 4 show that this limit can be reached when surface diffusion is negligible, which would be the case with a more physically realistic model. Because this affects both the macroporous and polymer-grafted systems, the two transport rates can still be readily compared, which in this study is of greater importance that modeling the fine details of the pore surface with high accuracy.

Discussion

The multiscale simulations show that in a polymer-grafted adsorbent, the protein transport rate is accelerated when partitioning from the bulk into the polymer-filled pore space is very favorable, as illustrated in Figure 5. Under these conditions, the increase in c_p more than offsets the decrease in protein diffusion due to interactions with the charged polymers, leading to a large $\partial c_p/\partial r$ driving force for intraparticle transport. When binding conditions are less favorable, the transport rate is not enhanced in the polymer-grafted system because the increase in c_p is insufficient to affect the overall mass transfer flux. The relationship between partitioning into the polymer-filled pore space and the transport rate could have implications for material design. Protein affinity for the charged polymers could be enhanced by either increasing the extent to which each graft is functionalized, or by grafting a higher density of polymers to the surface. However, an overly high graft density could negatively affect the total binding capacity if it significantly reduced protein adsorption to the pore surface, as is observed in our MD simulations. Greater flexibility of the polymer grafts might also increase the number of multivalent interactions that protein molecules

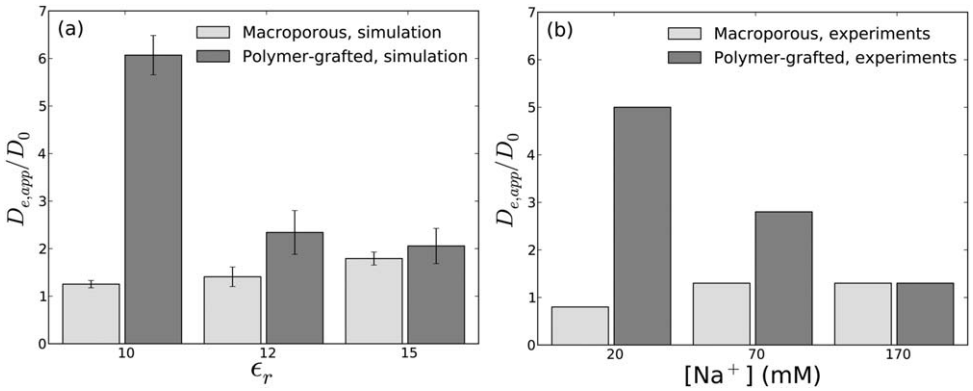

Figure 9. Multiscale simulation results (a) show that the effective transport rate of lysozyme, as measured by $D_{e,app}/D_0$, is enhanced in a polymer-grafted adsorbent under favorable binding conditions, which agrees qualitatively with previous experimental results (b) originally reported in Ref. 7. Error bars show the standard error of the mean.

can make with the polymers, and as a result, the amount of partitioning into the pore space.

In some systems, protein affinity for the polymer grafts and/or the underlying surface could also be affected by dispersion interactions or water-mediated hydrophobic interactions. By neglecting these in our simulations, we assume that the neutral protein residues and dextran monomers have approximately the same affinity for water as for each other, and that protein affinity for the adsorbent is dominated by the electrostatics of the overall net charge. The extent to which this approach can capture experimental trends when applied to different types of proteins will inform future modifications to the force field.

The geometry of the adsorbent pore could also affect the adsorption and diffusion of certain proteins. For large proteins, the curvature of the pore surface over long length scales may affect the number of molecules that can adsorb to the surface, just as the surface roughness on short length scales affects lysozyme's adsorption. The surface geometry can also affect the structure of the grafted polymer phase as has been shown in a previous MD study,[35] which would likely impact the protein's diffusion through the polymers and accessibility to the surface. These effects may not be significant for lysozyme due to its relatively small size, however, various pore geometries should be considered in MD simulations of larger proteins.

Simulations of other proteins will also be necessary to determine if our model can predict the correct shape of the intraparticle concentration profile in a given adsorbent material. Confocal laser scanning microscopy images for different proteins and adsorbents have shown qualitatively different profiles for certain proteins in open-pore and polymer-grafted ion exchange particles under transient adsorption conditions, suggesting that transport occurs via different diffusion mechanisms.[36,37] Sharp adsorbed protein concentration profiles have been observed for strong binding conditions in open-pore materials, indicating that surface diffusion plays little or no role, as that mechanism would lead to more diffuse adsorption profiles. Conversely, diffuse profiles have been obtained for some proteins in polymer-grafted materials, indicating that adsorbed protein molecules remain mobile. These differences have not been observed for lysozyme in light microscopy experiments,[5] nor are they observed in the simulation results presented here. However, preliminary numerical simulations (not shown) do predict more diffuse profiles for lysozyme when a greater percentage of the protein within the pore is associated with the charged polymers, where diffusion is much faster than on the surface.

Conclusions

A multiscale modeling approach is developed to estimate the adsorption capacity and transport rate of protein in IEC media with different pore architectures, based on the molecular-level details of the system. Coarse-grained MD simulations are used to determine the partitioning and diffusion of protein molecules within the adsorbent pore, and based on these molecular behaviors, numerical simulation of mass transfer over longer scales is used to quantify the effective transport rate.

A series of numerical simulations were initially performed to predict how different levels of protein diffusion and partitioning on the surface and in the polymers affect the effective transport rate in macroporous and polymer-grafted adsorbents. Based on these results, we determined molecular model parameters for the agarose surface, the charge content per grafted polymer, and the strength of electrostatics under favorable binding conditions that lead to simulated transport rates that agree with previous experiments. These model parameters were used to study how varying the strength of electrostatics affects adsorption behaviors.

Consistent with previous experiments, we observe that the binding capacities of both adsorbents and the enhancement in the transport rate of the polymer-grafted adsorbent decrease as electrostatic interactions become weaker. The enhanced transport in the polymer-grafted system when electrostatics are strong is attributed to favorable protein partitioning into the polymer-filled pore space, and the fact that the protein associated with the charged polymers retains significant diffusional mobility. Whereas adsorption to the surface decreases the protein's diffusivity by up to three orders of magnitude relative to D_0, association with the charged polymers leads to only a 33% reduction when electrostatics are strong. The simulations show that the macroporous and polymer-grafted adsorbents have similar overall binding capacities under favorable binding conditions, in contrast with experiments showing a 10–20% higher binding capacity

for lysozyme in a dextran-grafted adsorbent vs. a macroporous material. This modeling approach can be extended in a straightforward manner to proteins and adsorbents with different characteristics to better understand how molecular details influence macroscopic protein adsorption behaviors, and to utilize this understanding to help design efficient separation processes in the future.

Acknowledgment

The authors acknowledge NSF grant CBET-1032727 for funding of this research.

Literature Cited

1. Sommerfeld S, Strube J. Challenges in biotechnology production-generic processes and process optimization for monoclonal antibodies. *Chem Eng Process*. 2005;44:1123–1137.
2. Carta G, Jungbauer A. *Protein Chromatography: Process Development and Scale-Up*. Weinheim, Germany: Wiley-VCH Verlag GmbH & Co. KGaA, 2010.
3. Thömmes J. Investigations on protein adsorption to agarose-dextran composite media. *Biotechnol Bioeng*. 1999;62:358–362.
4. Müller W. New ion exchangers for the chromatography of biopolymers. *J. Chromatogr. A*. 1990;510:133–140.
5. Stone MC, Carta G. Protein adsorption and transport in agarose and dextran-grafted agarose media for ion exchange chromatography. *J. Chromatogr. A*. 2007;1146:202–215.
6. Bowes BD, Koku H, Czymmek KJ, Lenhoff AM. Protein adsorption and transport in dextran-modified ion-exchange media. I: adsorption. *J. Chromatogr. A* 2009;1216:7774–7784.
7. Stone MC, Tao Y, Carta G. Protein adsorption and transport in agarose and dextran-grafted agarose media for ion exchange chromatography: effect of ionic strength and protein characteristics. *J. Chromatogr. A*. 2009;1216:4465–4474.
8. Lenhoff AM. Protein adsorption and transport in polymer-functionalized ion-exchangers. *J. Chromatogr. A*. 2011;1218:8748–8759.
9. Heitzig M, Sin G, Glarborg P, Gani R. A computer-aided framework for regression and multi-scale-modelling needs in innovative product-process engineering. *Comput-Aided Chem Eng Ser*. 2010;28:379–384.
10. Lenhoff AM. Multiscale modeling of protein uptake patterns in chromatographic particles. *Langmuir*. 2008;24:5991–5995.
11. Dziennik SR, Belcher EB, Barker GA, DeBergalis MJ, Fernandez SE, Lenhoff AM. Nondiffusive mechanisms enhance protein uptake rates in ion exchange particles. *Proc Natl Acad Sci USA*. 2003;100: 420–425.
12. Ubiera AR, Carta G. Radiotracer measurements of protein mass transfer: kinetics in ion exchange media. *Biotechnol J*. 2006;1:665–674.
13. Latour RA. Molecular simulation of protein-surface interactions: benefits, problems, solutions, and future directions (Review). *Biointerphases*. 2008;3:FC2–FC12.
14. Zhang L, Sun Y. Molecular simulation of adsorption and its implications to protein chromatography: a review. *Biochem Eng J*. 2010;48: 408–415.
15. Zhang X, Wang JC, Lacki KM, Liapis AI. Molecular dynamics simulation studies of the transport and adsorption of a charged macromolecule onto a charged adsorbent solid surface immersed in an electrolytic solution. *J Colloid Interface Sci*. 2004;277:483–498.
16. Dismer F, Hubbuch J. 3D structure-based protein retention prediction for ion-exchange chromatography. *J Chromatogr A*. 2010;1217: 1343–1353.
17. Kubiak-Ossowska K, Mulheran PA. Mechanism of hen egg white lysozyme adsorption on a charged solid surface. *Langmuir*. 2010;26: 15954–15965.
18. Liang J, Fieg G, Keil FJ, Jakobtorweihen S. Adsorption of proteins onto ion-exchange chromatographic media: a molecular dynamics study. *Ind Eng Chem Res*. 2012;51:16049–16058.
19. Riccardi E., Wang JC., Liapis AI. A molecular dynamics study on the transport of a charged biomolecule in a polymeric adsorbent medium and its adsorption onto a charged ligand *J Chem Phys*. 2010;133:084904.
20. Riccardi E, Wang JC, Liapis AI. Molecular modeling of polymeric adsorbent media: the effects of counter-ions on ligand immobilization and pore structure. *J Sep Sci*. 2012;35:3073–3083.
21. Freed AS, Garde S, Cramer SM. Molecular simulations of multimodal ligand protein binding: elucidation of binding sites and correlation with experiments. *J Phys Chem B*. 2011;115:13320–13327.
22. Hess B, Kutzner C, Spoel D, Lindahl E. GROMACS 4: algorithms for highly efficient, load-balanced, and scalable molecular simulation. *J Chem Theory Comput*. 2008;4:435–447.
23. Basconi JE, Shirts MR. Effects of temperature control algorithms on transport properties and kinetics in molecular dynamics simulations. *J Chem Theory Comput*. 2013;9:2887–2899.
24. Tyn TM, Gusek TW. Prediction of diffusion coefficients of proteins. *Biotechnol Bioeng*. 1990;35:327–338.
25. Barker JA. Reaction field, screening, and long-range interactions in simulations of ionic and dipolar systems. *Mol Phys*. 1994;83:1057–1064.
26. Artymiuk PJ, Blake CCF, Rice DW, Wilson KS. The structures of the monoclinic and orthorhombic forms of hen egg-white lysozyme at 6 Å resolution. *Acta Crystallogr Sect B: Struct Crystallogr Cryst Chem*. 1982;38:778–783.
27. Tozzini V. Coarse-grained models for proteins. *Curr Opin Struct Biol*. 2005;15:144–150.
28. Jorgensen WL, Tirado-Rives J. The OPLS [optimized potentials for liquid simulations] potential functions for proteins, energy minimizations for crystals of cyclic peptides and crambin. *J Am Chem Soc*. 1988;110:1657–1666.
29. Binder K. *Monte Carlo and Molecular Dynamics Simulations in Polymer Science*. New York: Oxford University Press, 1995; 125–194.
30. Rief M, Fernandez JM, Gaub HE. Elastically coupled two-level systems as a model for biopolymer extensibility. *Phys Rev Lett*. 1998; 81:4764–4767.
31. Snoussi K, Halle B. Protein self-association induced by macromolecular crowding: a quantitative analysis by magnetic relaxation dispersion. *Biophys J*. 2005;88:2855–2866.
32. Bielecki S, Polak J, Tramper J. *Food Biotechnology (Progress in Biotechnology)*. Amsterdam: Elsevier Science, 2000.
33. Kim YM, Kimura A, Kim D. Novel quantitative method for the degree of branching in dextran. *Food Sci Biotechnol*. 2011;20:537–541.
34. Schiesser WE. *The Numerical Method of Lines: Integration of Partial Differential Equations*. San Diego: Academic Press, Inc., 1991.
35. Riccardi E, Wang JC, Liapis AI. Rational surface design for molecular dynamics simulations of porous polymer adsorbent media. *J Phys Chem B*. 2008;112:7478–7488.
36. Tao Y, Almodóvar EX, Carta G, Ferreira G, Robbins D. Adsorption kinetics of deamidated antibody variants on macroporous and dextran-grafted cation exchangers. *III. Microscopic studies. J Chromatogr A*. 2011;1218:8027–8035.
37. Pérez-Almodóvar EX, Tao Y, Carta G. Protein adsorption and transport in cation exchangers with a rigid backbone matrix with and without polymeric surface extenders. *Biotechnol Prog*. 2011;27: 1264–1272.

Manuscript received June 5, 2014, and revision received Aug. 9, 2014.